Intraction of In-Plane Shear and Flexure in Masonry Walls with Unbonded Longitudinal Reinforcement

Alok Madan[1], Andrei M. Reinhorn[2] and John B. Mander[3]

A reinforced masonry shear wall subjected to in-plane lateral and axial loads behaves as a two-dimensional continuum in a state of plane stress. In a grouted masonry shear wall with longitudinal steel reinforcement, bond between masonry and steel enables effective transfer of forces between the longitudinal steel rebars and adjoining masonry through shear stresses, commonly known as bond stresses, acting at the surface of the rebar. The load-resisting mechanism of the wall can be explained using the traditional analogy of a parallel chord pin-jointed truss [Park et al. (1975), Collins et al. (1991)] shown in Figure 1(a). Force in the longitudinal tension chord of a parallel chord truss changes at the discrete pin-joints due to forces entering the joints from the diagonal compression struts. Analogously, in a two-dimensional reinforced masonry wall continuum, forces in the longitudinal rebars change continuously from point to point along the rebar length due to the diagonal compression field in the masonry [Figure 1(a)]. The change in the longitudinal steel tensile force, which also equals the change in the longitudinal component of masonry compressive force, produces change in the internal resisting moment (couple) required for balancing the external shear force. This mode of shear resistance, termed as 'beam action' [Figure 1(a)], is viable only in the presence of bond stresses.

In an ungrouted masonry shear wall with longitudinal (vertical) steel reinforcement, forces in the longitudinal reinforcing bars cannot change along the length because of the complete absence of bonding between the reinforcing steel and adjacent masonry. As a result, 'beam action' is replaced by an alternative mechanism known as the 'arch action' after development of a flexural crack at the base. In arch action, external shear is resisted by an inclined internal compression field in the masonry [Figure 1(b)]. The change in internal resisting couple along the height, required for the shear resistance, is

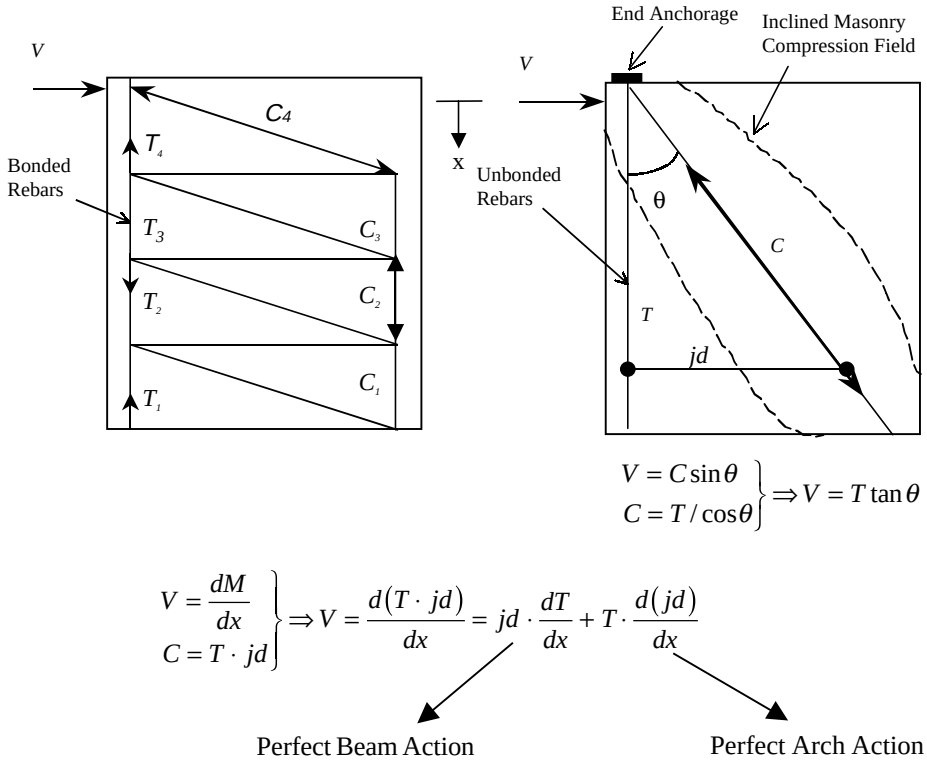

Figure 1—Shear Resisting Mechanism of a Masonry Wall – Bonded vs. Unbonded Reinforcement

[1] Assistant Professor, Department of Civil Engineering, Indian Institute of Technology, New Delhi, India
[2] Professor and Chairman, Department of Civil Engineering, State University of New York, Buffalo, NY 14260
[3] Associate Professor, Department of Civil Engineering, State University of New York, Buffalo, NY 14260

developed in this case by the longitudinal variation of the lever arm (*jd*) between the tensile steel force and compressive masonry force resultants due to inclined trajectory of the compressive force ("tie-strut" mechanism).

Past research studies demonstrated that the relative contribution of flexure and shear to the lateral load behavior of reinforced masonry shear walls is governed by the height-to-width ratio (aspect ratio) of the wall [Shing et al. (1989), Hart (1991)]. Generally, flexural behavior dominates in a slender wall (i.e., a flexure-critical wall), while shear deformations govern the response of a short wall (i.e., a shear-critical member). In a slender masonry shear wall with ungrouted (unbonded) vertical reinforcement, flexural cracking of the mortar bed joint between the wall base and foundation results in a partial loss of connectivity at the base, causing a part of the wall to separate and lift up from the foundation. Uplift initiates when the overturning moment due to lateral load exceeds the total restoring moment offered by the vertical dead load on the wall base [Priestley (1991)] and the tie-down forces exerted by vertical reinforcing bars.

The analysis of flexible structures undergoing uplift is a complex problem, since uplift is ideally a rigid body motion of the structure under stable dynamic equilibrium with no increase in the internal strain energy (zero energy mode of response). In the case of flexible structures in equilibrium under external forces, rigid body motion may coexist with strain deformations on partial loss of end restraint. A detailed survey of existing analytical models of uplift in flexible structures on flexible foundations is presented by Madan (1996) and Madan et al. (1998). However, the problem of masonry shear walls with ungrouted (unbonded) verical reinforcement is further complicated by the fact that tie-down forces in unbonded reinforcing bars depend on displacements of the wall boundary. In a squat masonry wall with unbonded vertical (longitudinal) reinforcement, the lateral load produces sliding of the wall if the load exceeds the shear capacity at the wall base-foundation interface. In either case (uplift or sliding), flexural and shear deformations in the wall are accompanied by a rigid body motion of the wall. In masonry walls with grouted (bonded) longitudinal reinforcement, bonding between the longitudinal steel rebars and masonry restrains this rigid body motion.

A review of current analytical models for lateral load behavior of ungrouted reinforced and post-tensioned masonry shear walls was performed by Madan, Reinhorn et al. (1996). That review indicated that a common practice in strength analysis of reinforced masonry is to assume that the strain in a reinforcing bar at any section is compatible with the masonry strain at the location of the rebar in that section. As a consequence, the response of any section can be determined from force equilibrium and displacement compatibility of that section only (independent of the member response), using a suitable numerical technique based on a layered model of the section or a "layer-by-layer" modeling approach [Collins et al. (1990)]. Vecchio and Collins (1988) presented a layered section model (fiber element model) to perform detailed inelastic analysis of a reinforced concrete section subjected to combined moment and shear. This analysis method, referred to as the "dual section analysis", enables determination of the complete nonlinear shear and flexural response of a given section in a reinforced concrete member based on equilibrium and compatibility of that section only. The "dual section analysis" procedure is discussed in detail by Vecchio and Collins (1988).

In reinforced masonry shear walls with unbonded longitudinal reinforcement, however, strains in the reinforcing bars at any section cannot be directly related to the deformations of that section [Madan, Reinhorn et al. (1996)]. In this case, the steel rebar strains depend on the relative displacements of the end anchorages [Park et al. (1975)] and are thus governed by displacements of the wall boundary. As a result, analysis of the sectional response in masonry shear walls with unbonded longitudinal reinforcement cannot be completed at the sectional level without considering the structural response of the entire wall [Madan, Reinhorn et al. (1996)]. In view of these differences, the available analysis techniques are deficient in predicting the in-plane lateral load response of masonry shear walls with unbonded reinforcement. The present paper is part of a series based on the results of a research program that investigates the in-plane behavior of masonry shear walls with unbonded longitudinal reinforcement with or without prestress. An integrated analytical method, based on a micro-element model, is presented for determining the nonlinear force-displacement envelope as well as detailed stress and strain response of masonry shear walls with unbonded longitudinal reinforcement under the action of an in-plane lateral load. The proposed analysis technique accounts for the interaction of flexure, shear and uplift in such walls under in-plane lateral loading. Further, the modeling approach is generalized since the model can also be implemented for analysis of masonry shear walls with bonded reinforcement by making minor modifications in the numerical procedure.

ANALYTICAL MODELING

Consider a reinforced concrete masonry shear wall [Figure 2(a)] of height H, length L and width b under the action of an in-plane lateral load F with N_b number of unbonded reinforcing bars of cross-sectional areas A_{sj} located at coordinates y_j from the center of wall section [Figure 2(e)]. In each case, the subscript j refers to the j^{th} bar. Horizontal steel reinforcement of area A_h is provided in the wall for shear resistance at an effective spacing s_h along the height. Details of analytical modeling of the in-plane response of the wall are presented in this part of the paper. Idealizing the wall as a cantilever structure fixed at the base, the vertical axial force P_x, in-plane bending moment M_z, and lateral

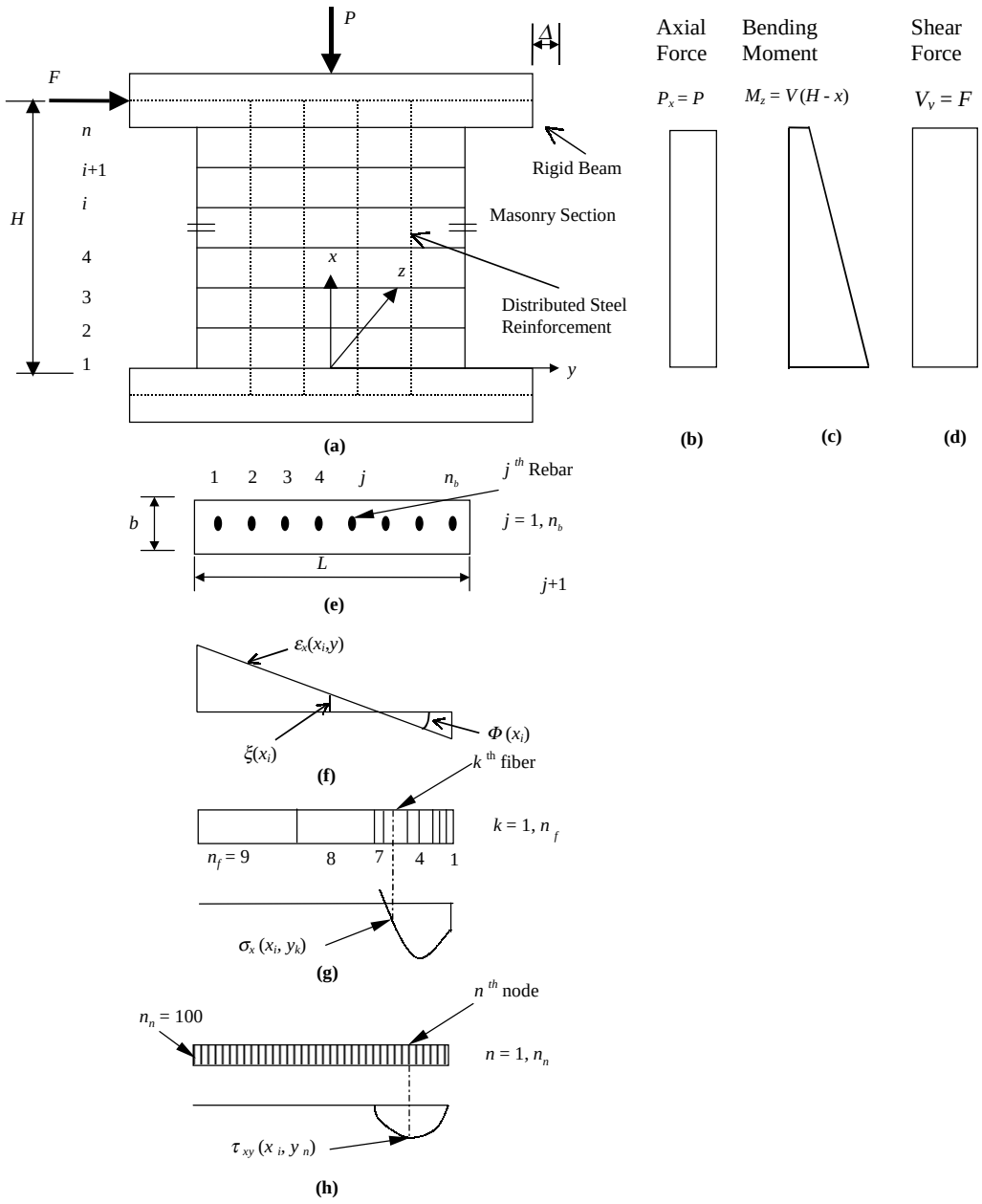

Figure 2—Concrete Masonry Shear Wall with Distributed Vertical Reinforcement: Geometry, Behavior and Modeling

shear force V_y acting on any transverse section can be determined from mechanics. Their variations along the x direction are shown in Figures 2(b), 2(c) and 2(d), respectively. The internal forces at any section i located at height x_i from the base may be related to the external forces by examining the static force and moment equilibrium of the section as follows:

$$P_x(x_i) = C(x_i) - T_s(x_i) \quad \textbf{(1)}$$

$$M_z(x_i) = M(x_i) - M_s(x_i) \quad \textbf{(2)}$$

$$V_y(x_i) = V(x_i) + V_s(x_i) \quad \textbf{(3)}$$

where $C(x_i)$ and $T_s(x_i)$ are the internal compressive forces in masonry and internal tensile forces in steel, respectively, in the vertical x direction; $M(x_i)$ and $M_s(x_i)$ are the internal resisting moments due to masonry and steel, respectively, about the z direction; $V(x_i)$ is the internal shear force in the horizontal y direction due to masonry's shear resistance (diagonal cracking strength) and shear reinforcement; while $V_s(x_i)$ is the shear resistance of masonry in the y direction due to dowel action of longitudinal steel is the shear resistance of masonry in the y direction due to dowel action of longitudinal steel.

Mechanics of Materials

Masonry - The stress-strain state in the masonry element or fiber was solved using modified compression field

theory [Collins et al. (1990)]. The theory, which was originally developed for concrete by Vecchio and Collins (1988), relates the average stresses and average strains in a cracked or uncracked reinforced element [Figure 3(a)] under an external loading. The theory is based on force equilibrium and displacement compatibility. Using realistic uniaxial stress-strain relationships for concrete and steel, the modified compression field theory provides a sound analytical approach for obtaining a unique solution of the complete biaxial stress and strain response of the element for any two known values of stresses and strains. The analysis involves an iterative numerical procedure that accounts for strain softening effects, local stress conditions at crack locations and variation in the angle of inclination of the concrete compression field. Details of the theory and numerical procedure may be found elsewhere [Collins et al. (1990), Madan (1996)]. The modified compression field theory is adopted in the present study for modeling the biaxial stress-strain response of a concrete masonry element.

The uniaxial stress-strain behavior of masonry may be defined using suitable constitutive models. The equation proposed by Mander et al. (1988) was used to model the relationship between stress, f_m, and strain, ε_m, for masonry in uniaxial compression. The equation generates a single continuous curve for modeling the experimentally-observed stress-strain relationship for confined or unconfined concrete in uniaxial compression [Figure 3(b)] and may be written as:

$$f_m = \frac{f'_m \cdot x \cdot r}{r - 1 + x^r} \qquad \textbf{(4)}$$

$$\text{where } x = \frac{\varepsilon_m}{\varepsilon'_m};\ r = \frac{E_m}{E_m - E_{\text{sec}}};\quad E_m = \frac{df_m}{d\varepsilon_m}(\varepsilon_m = 0) \text{ and } E_{\text{sec}} = \frac{f'_m}{\varepsilon'_m} \qquad \textbf{(5)}$$

in which f'_m is the peak compressive stress and ε'_m is the corresponding strain; E_m is the initial slope of the stress-strain curve and E_{sec} is the slope of the secant to the peak stress.

The stress-strain relationship suggested by Collins et al. (1990) was used for masonry in uniaxial tension. The proposed relation between tensile stress, f_{mt}, and tensile strain, ε_{mt}, may be expressed as follows:

$$\text{if} \quad \varepsilon_m \le \varepsilon_{cr} \quad \text{then} \quad f_{mt} = E_m \varepsilon_{mt} \qquad \textbf{(6a)}$$

$$\varepsilon_m > \varepsilon_{cr} \quad \text{then} \quad f_{mt} = \frac{\alpha_1 \alpha_2 f_{cr}}{1 + \sqrt{500.\varepsilon_{mt}}} \qquad \textbf{(6b)}$$

where ε_{cr} is the cracking strain; f_{cr} is the cracking stress or modulus of rupture for masonry; α_1 is a factor accounting for bond characteristics of the steel reinforcement and α_2 is a factor depending on the nature of loading. Thus, a linearly elastic stress-strain relation is specified for masonry in tension until the cracking strain is reached [Figure 3(b)]. At higher strains, the cracked masonry may resist tensile stresses due to tension stiffening, depending on the bond characteristics of the reinforcement. With unbonded reinforcement, however, the masonry is unable to resist tensile stresses after cracking and, thus, fails in tension. Therefore, $\alpha_1 = 0$ for masonry walls with unbonded longitudinal reinforcement.

Reinforcing Steel - In general, the masonry shear wall is provided with horizontal steel for shear reinforcement as well as vertical steel for flexural reinforcement.

Horizontal Steel: For modeling purposes, the total horizontal shear reinforcement was assumed smeared along the wall height to provide an effective horizontal steel area equal to A_h/s_h per unit height of the wall. Smearing of horizontal steel precludes evaluation of local variations in horizontal stresses and strains in the vicinity of discrete crack locations. However, the foregoing approach, proposed by Vecchio and Collins (1988) for reinforced concrete panels, is efficient and accurate for the purpose of evaluating the average horizontal stresses and strains (averaged over a finite height) in the steel and masonry at a given location in the wall. Since the horizontal shear reinforcement is fully bonded to the neighboring masonry, the horizontal steel strains and masonry strains may be related by the following compatibility equation:

$$\varepsilon_h(x_i, y) = \varepsilon_y(x_i, y) \qquad \textbf{(7)}$$

in which $\varepsilon_h(x_i, y)$ is the horizontal steel strain in the i^{th} section at coordinate y and ε_y is the normal strain in the masonry in the y direction [Figure 3(a)].

The equilibrium of any longitudinal section requires that

$$\sigma_h(x_i, y) = \frac{b_w s_h}{A_h} \sigma_y(x_i, y) \qquad \textbf{(8)}$$

in which b_w equals the wall width b, $\sigma_h(x_i, y)$ is the horizontal steel stress in the i^{th} section at coordinate y and σ_y is the normal stress in masonry in the y direction [Figure 3(a)].

Vertical Steel: As discussed previously, if the vertical (longitudinal) reinforcement is fully bonded to the neighboring masonry, the strain $\varepsilon_s(x_i, y_j)$ in the vertical rebar j at any cross-section i is commonly assumed to be equal to the masonry strain at the location of the rebar in that section. The compatibility condition may be expressed as:

$$\varepsilon_s(x_i, y_j) = \varepsilon_p + \varepsilon_x(x_i, y_j) \qquad \textbf{(9)}$$

in which ε_p is the strain in the masonry resulting from the applied vertical prestress in the rebar.

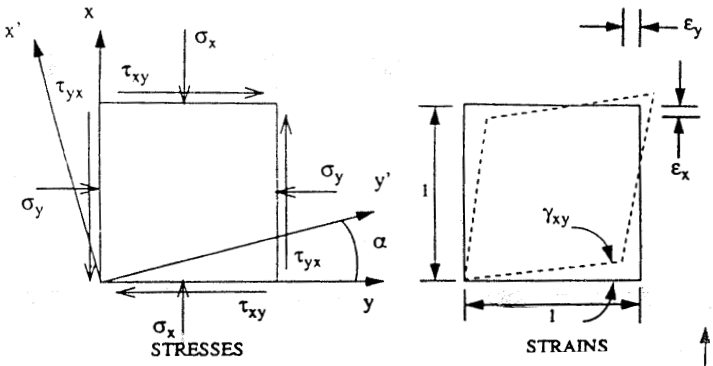

(a) Average Stresses and Strains in Differential Masonry Element

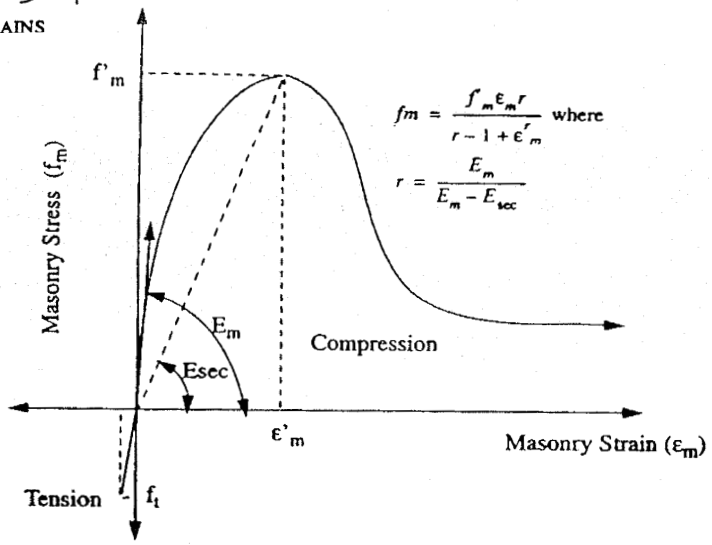

(b) Constitutive Model for Masonry

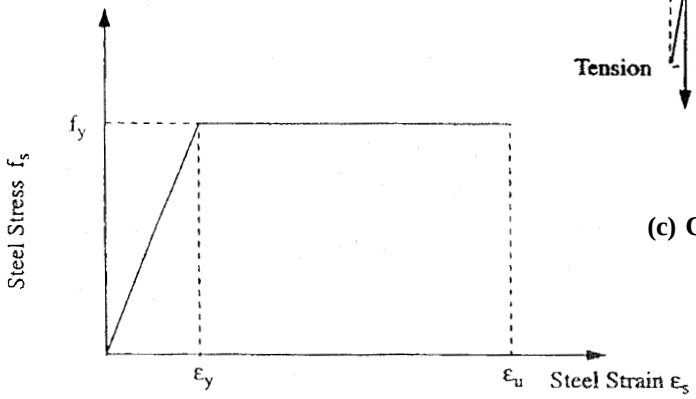

(c) Constitutive Model for Steel

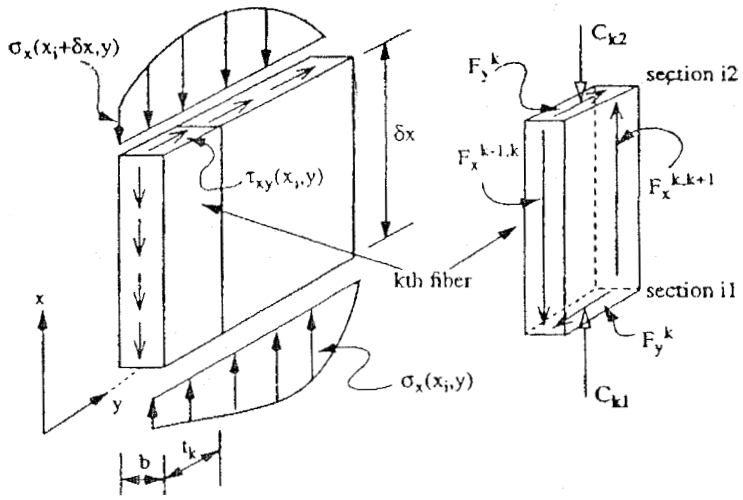

(d) Longitudinal Equilibrium of Masonry Fiber Element

Figure 3—Micro Mechanics of Masonry Wall and Material Properties

In the case of masonry shear walls with unbonded vertical reinforcement, the foregoing compatibility relation is not admissible, since the longitudinal strain in the unbonded vertical steel reinforcing bar is governed by the relative displacement of the end anchorages and, thus, cannot be expressed as an independent function of the masonry strain at any single location. In this case, a compatibility condition exists between the unbonded vertical steel strains and the wall displacements. Assuming that the rebars are anchored at the upper end in the top beam and at the lower end in the foundation beam [Figure 2(a)], the relative longitudinal displacement of the end anchorages of the j^{th} rebar may be closely approximated as the vertical displacement of the wall at top end of the rebar. The uniaxial longitudinal strain $\varepsilon_s(y_j)$ in the j^{th} unbonded rebar due to wall displacement may be thus calculated as:

$$\varepsilon_s(y_j) = \varepsilon_p + \frac{u(H, y_j)}{H} \quad \textbf{(10)}$$

where $u(x, y)$ is the vertical displacement in the longitudinal x direction at coordinates (x, y).

A bilinear elastic-plastic stress-strain curve [Figure 3(c)] was adopted for both bonded and unbonded steel. Thus, the steel stress, f_s, is functionally related to strain ε_s as:

$$f_s(\varepsilon_s) = E_s^0 \cdot \varepsilon_s \le f_y \quad \textbf{(11)}$$

where E_s^0 and f_y are the modulus of elasticity and yield strength of steel, respectively.

In case of bonded horizontal steel, the bilinear relation Equation 11 was used to model uniaxial tensile as well as compressive stress-strain behavior. However, the unbonded vertical reinforcing bars were assumed to be ineffective in compression. This is a reasonable assumption in the absence of any bracing along the height of the wall.

Modeling of Flexural and Shear Response

The in-plane stress response of the wall was modeled on the basis of following assumptions:

1. The distribution of normal strain $\varepsilon_x(x_i, y)$ in masonry at any section i is linear along the depth of the section (in the y direction), i.e., plane sections remain plane.
2. The normal strain $\varepsilon_x(x_i, y)$ and shear stress $\tau_{xy}(x_i, y)$ in a masonry element located at coordinate y in the i^{th} section uniquely define the state of stress and strain in that element, according to modified compression field theory.
3. The shear stress distribution $\tau_{xy}(x, y)$ at two sections separated by a small distance ∂x is the same, i.e., $\tau_{xy}(x_i, y) = \tau_{xy}(x_i + \partial x, y)$ if $\partial x << H$.

From assumption 1 above, the normal masonry strain in any section i at distance y from the center [Figure 2(f)] may be expressed as:

$$\varepsilon_x(x_i, y) = \xi(x_i) + y \cdot \Phi(x_i) \quad \textbf{(12)}$$

in which $\xi(x_i)$ is the normal strain in masonry at the center of i^{th} section and $\Phi(x_i)$ is the angle of inclination of the linear strain profile at the i^{th} section, also referred to as the flexural curvature of that section [Figure 2(f)].

The internal forces in equilibrium equations 1, 2 and 3 may be calculated as:

$$C(x_i) = \int_{-L/2}^{L/2} \sigma_x(x_i, y) \cdot b \cdot dy \quad \textbf{(13)}$$

$$T_s(x_i) = \sum_{j=1}^{N_b} E_s(\varepsilon_s) \cdot A_{sj} \cdot \varepsilon_s(y_j) \quad \textbf{(14)}$$

$$V(x_i) + V_s(x_i) = \int_{-L/2}^{L/2} \tau_{xy}(x_i, y) \cdot b \cdot dy \quad \textbf{(15)}$$

while the internal moments may be obtained as

$$M(x_i) = \int_{-L/2}^{L/2} y \cdot \sigma_x(x_i, y) \cdot b \cdot dy \quad \textbf{(16)}$$

$$M_s(x_i) = \sum_{j=1}^{N_b} y_j \cdot E_s(\varepsilon_s) \cdot A_{sj} \cdot \varepsilon_s(y_j) \quad \textbf{(17)}$$

in which $E_s(\varepsilon_s)$ is the slope of the secant (secant modulus) to the point on the stress-strain curve of steel corresponding to strain ε_s and $\sigma_x(x_i, y)$ is the normal stress in a masonry element at coordinate y in the i^{th} section. From assumption (2) above, $\sigma_x(x_i, y)$ can be uniquely determined for a given normal strain $\varepsilon_x(x_i, y)$ and shear stress $\tau_{xy}(x_i, y)$, i.e.,

$$\sigma_x(x_i, y) = \sigma_x\left[\varepsilon_x(x_i, y), \tau_{xy}(x_i, y)\right] \quad \textbf{(18)}$$

The longitudinal equilibrium of the section [Figure 3(d)] requires that the normal stress $\sigma_x(x_i, y)$ and shear stress $\tau_{xy}(x_i, y)$ distributions are related as:

$$\tau_{xy}(x_i, y) = \lim_{\partial x \to 0} \frac{\int_{-L/2}^{y} \left[\sigma_x(x_i + \partial x, \bar{y}) - \sigma_x(x_i, \bar{y})\right] \cdot b \cdot d\bar{y}}{b \cdot \partial x} + \frac{\sum_{j=1}^{j} E_s(\varepsilon_s) \cdot A_{s\bar{j}} \cdot \varepsilon_s\left(x_i + \partial x, y_{\bar{j}}\right) - \varepsilon_s\left(x_i, y_{\bar{j}}\right)}{b \cdot \partial x} \quad \textbf{(19)}$$

in which j is the rebar number such that $y_j \le y \le y_{j+1}$.

In Equation 19, the first term accounts for shear stresses due to masonry shear resistance including the effect of horizontal shear reinforcement, while the second term represents the contribution of dowel action provided by longitudinal reinforcement. In the case of unbonded longitudinal reinforcement, strains in the unbonded rebars do not vary along the length of the rebar. As a result, the shear resistance due to dowel action is not mobilized and Equation 19 reduces to:

$$\tau_{xy}(x_i, y) = \lim_{\partial x \to 0} \frac{\int_{-L/2}^{y} \left[\sigma_x(x_i + \partial x, \bar{y}) - \sigma_x(x_i, \bar{y})\right] \cdot b \cdot d\bar{y}}{b \cdot \partial x} \quad \textbf{(20)}$$

Modeling of Uplift Behavior

Since strains in the unbonded longitudinal reinforcing bars depend on the relative dispacements of the end anchorages, the steel strains are functions of masonry strain deformations as well as uplift displacements of the wall. As discussed earlier, uplift is a dynamic phenomenon with a complex dependence on many governing factors, including the overturning moment at the base $M_z(x_1)$, wall aspect ratio or height to length H / L ratio, axial load $P_x(x_1)$ at the base, prestressing force in the vertical unbonded rebars, wall weight W and time rate of change of the overturning moment. Progressive uplift of the wall base causes a reduction in the contact area between the base and foundation thus producing a stress concentration (penetration) in the contact region. Therefore, compatibility exists between the magnitude of rigid body uplift and strains at the base. The following assumptions were made to model the uplift response of the masonry shear walls with unbonded vertical reinforcement:

(a) After initiation of flexural cracking at the base, rigid body rotation θ of the shear wall (Figure 4) occurs along with strain deformations under lateral loading. The instantaneous center of this rigid body rotation was assumed as the point of action of the resultant of compressive stress distribution (the point of reaction C) at the base.

(b) The incremental displacement, $\partial\delta_c$, due to the stress concentration at the extreme compression fiber (toe of the wall) can be related by geometry to the incremental angle of uplift, $\partial\theta$, between the uplifted base and foundation at the point of separation (Figure 4).

(c) The incremental vertical displacement $\partial\delta_c$ at the extreme compression fiber can be averaged over a finite height, H_p, to obtain the incremental normal compressive strain at that location $\partial\varepsilon_x$ (x_1, $L / 2$). The height, H_p, termed as the average height of the stressed zone in this paper, depends on parameters that govern rigid body motion and were mentioned earlier. Intuitively, however, the average height of the stressed zone, H_p, at the extreme compression fiber (above the toe) of the wall bears a direct correlation to both the axial (vertical) load on the wall and the wall aspect (height to length) ratio. A physical interpretation of the relationship may be realized by noting that the greater the axial load or aspect ratio, the higher the inclination of the internal masonry compression field towards the vertical axis of the wall.

Using the foregoing assumptions and geometry shown in Figure 4, a compatibility relationship can be derived between the increments in rigid body rotation, θ, of the wall and curvature, $\Phi(x_1)$, at the base in terms of wall length (L), contact length (d), distance (d_c) of the centroid of compressive stress distribution (point of reaction C) at the base from the extreme compression fiber, and the average height of the stressed zone (H_p) at the extreme compression fiber. Detailed derivation of the compatibility condition is presented by Madan et al. (1998) and only the proposed compatibility equation is included here:

$$\partial\theta = 0 \qquad \text{if } \varepsilon(x_1, -L/2) \geq \varepsilon_{cr} \quad \textbf{(21a)}$$

$$\partial\theta = \frac{H_p(L-d)}{(L-d_c)}\partial\Phi(x_1); \text{ if } \varepsilon(x_1, -L/2) < \varepsilon_{cr} \quad \textbf{(21b)}$$

in which ε_{cr} is the cracking strain for masonry and d is the instantaneous contact length at the base may be estimated as:

$$d = \frac{L}{2} + \frac{\xi(x_1)}{\Phi(x_1)} \quad \textbf{(22)}$$

The instantaneous location of the compressive stress resultant C may be calculated as:

$$y_c = \frac{M(x_1)}{C(x_1)} \quad \textbf{(23)}$$

in which y_c is the y coordinate of point of action of the compressive stress resultant C.

Thus, the distance d_c of the stress resultant from the extreme compression fiber is given as:

$$d_c = \frac{L}{2} - y_c = \frac{L}{2} - \frac{M(x_1)}{C(x_1)} \quad \textbf{(24)}$$

Wall Displacements and Unbonded Rebar Strains

Idealizing the top of the wall as a free end and the base as a fixed end (cantilever end conditions), the vertical (longitudinal) in-plane displacement $u_s(x, y)$ due to strain de-

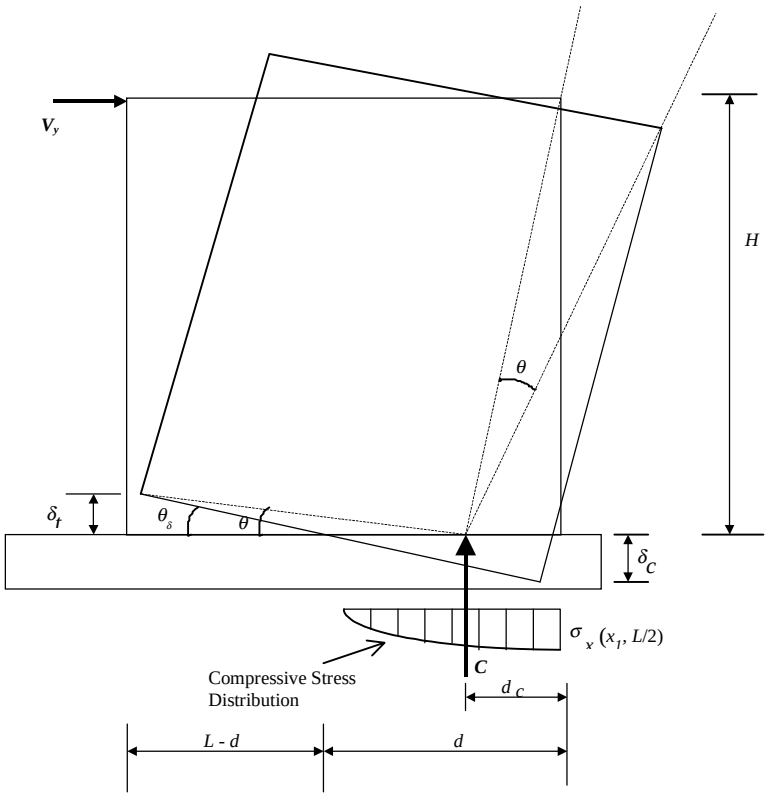

Figure 4—Displacement Compatibility of Uplift in Masonry Shear Walls with Unbonded Reinforcement

formations of the wall may be obtained as:

$$u_s(x, y) = \int_0^x \varepsilon_x(\bar{x}, y)d\bar{x} \quad \textbf{(25)}$$

The vertical in-plane displacement $u_r(x, y)$ due to rigid body uplift may be estimated from geometry (Figure 4) using assumption (a), Equation 23 and small angle approximation as:

$$u_r(x, y) = \theta \cdot (y_c - y) = \theta \cdot \left[\frac{M(x_1)}{C(x_1)} - y\right] \quad \textbf{(26)}$$

The total vertical in-plane displacement $u(x_i, y)$ of a point located at y coordinate in the i^{th} section may be calculated by adding the vertical displacement components due to strain deformations and uplift. Thus, from Equations 25 and 26,

$$u(x_i, y) = u_s(x_i, y) + u_r(x_i, y) = \int_0^{x_i} \varepsilon_x(x, y)dx + \theta \cdot \left[\frac{M(x_1)}{C(x_1)} - y\right] \quad \textbf{(27)}$$

The uniaxial longitudinal strain in j^{th} unbonded rebar $\varepsilon_c(y_j)$ may be calculated using Equations 10 and 27 as follows:

$$\varepsilon_s(y_j) = \varepsilon_p + \frac{\int_0^H \varepsilon_x(x, y_j)dx + \theta \cdot \left[\frac{M(x_1)}{C(x_1)} - y_j\right]}{H} \quad \textbf{(28)}$$

The strain deformation-produced lateral in-plane displacement $v_s(x_i, y)$ of a point located at y coordinate in the i^{th} section may be obtained as:

$$v_s(x_i, y) = \int_{0}^{x_i} \int_{-L/2}^{y} \gamma_{xy}\, dx + \int_0^{x_i} \Phi(x) \cdot (H - x)dx \quad \textbf{(29)}$$

Using assumption (a) and small angle approximation again, the uplift-produced lateral in-plane displacement $v_r(x_i, y)$ of location y in section i may be estimated as:

$$v_r(x_i, y) = \theta \cdot x_i \quad \textbf{(30)}$$

The total lateral in-plane displacement $v(x_i, y)$ is obtained by adding the two components from Equations 29 and 30 as:

$$v(x_i, y) = v_s(x_i, y) + v_r(x_i, y) = \int_{0}^{x_i} \int_{-L/2}^{y} \gamma_{xy}\, dx + \int_0^{x_i} \Phi(x) \cdot (H - x)dx + \theta \cdot x_i \quad \textbf{(31)}$$

The lateral displacement Δ at the top leeward edge ($x = H, y = L/2$) of the wall may be calculated from Equation 31 as:

$$\Delta = v(H, L/2) = \int_{0}^{H} \int_{-L/2}^{L/2} \gamma_{xy}\, dx + \int_0^{H} \Phi(x) \cdot (H - x)dx + \theta \cdot H \quad \textbf{(32)}$$

NUMERICAL ANALYSIS PROCEDURE

The biaxial stress distribution in the wall and non-linearity of component materials necessitate a numerical solution for the response. The numerical modeling and solution technique are described in this part of the paper.

Numerical Model of the Wall

The numerical solution of the inelastic lateral force-displacement response of masonry shear walls with unbonded reinforcement was obtained by discretizing the masonry shear wall into a finite number of sections, N_s, along the height [Figure 2 (a)]. Each of the finite sections was further discretized into differential elements or fibers along the length [Figure 2(g)]. The problem involves $3N_s + N_b + 1$ unknowns or variables which are: the masonry strain variables $\xi(x_i)$ and $\Phi(x_i)$ and shear stress distribution $\tau_{xy}(x_i, y)$ at each of the N_s sections, the strains $\varepsilon_s(y_j)$ in the N_b unbonded vertical rebars; and the rigid body rotation, θ, due to wall uplift. In order to obtain a solution, $3N_s$ equations are available from equilibrium (Equations 1, 2 and 3) of the N_s sections, N_b compatibility equations (Equations 28) are available for determining strain in each of the N_b unbonded rebars and 1 compatibility equation (Equation 21) is proposed for estimating the rigid body rotation θ. A number of shear stress distributions may satisfy these equations. However, a unique shear stress distribution is determined at each section by the longitudinal equilibrium equation (Equation 20).

Since strains in the unbonded longitudinal reinforcing bars $\varepsilon_s(y_j)$ are constant along the height of the wall, the internal steel force $T_s(x_i)$ and moment $M_s(x_i)$ are also invariant along the wall height (in the x direction). The proposed numerical analysis methodology is based on the idealization that the action of unbonded longitudinal reinforcing steel is statically equivalent to an unknown structural force, T_s, given by Equation 14 and an unknown structural moment, M_s, given by Equation 17. The structural force and moment act on the entire masonry wall and depend on the kinematics of the wall boundary [Madan, Reinhorn et al (1996)]. Dropping the argument x_i for these variables and rearranging Equations 1 and 2, the force equilibrium equations for any section *i* can be rewritten to express the steel force T_s and moment M_s as a structural force and moment respectively:

$$P_x(x_i) + T_s = C(x_i) \tag{33}$$

$$M_z(x_i) - M_s = M(x_i) \tag{34}$$

$$V_y(x_i) = V(x_i) + V_s(x_i) \tag{35}$$

The numerical analysis involves an iterative procedure in which the unknown structural force T_s and moment M_s due to the longitudinal reinforcing steel are estimated. In-plane strain deformations and uplift displacements of the masonry wall are evaluated for estimated values of the structural variables T_s and M_s. Strains, $\varepsilon_s(y_j)$, in the unbonded longitudinal rebars are calculated from the compatibility Equation 28 by numerical integration as follows:

$$\varepsilon_s(y_j) = \varepsilon_p + \frac{1}{H}\left\{\sum_{i=1}^{N_s} w_i \cdot \left[\xi(x_i) + y_j \cdot \Phi(x_i)\right]\cdot \Delta x_i\right\} + \frac{\theta}{H}\cdot\left[\frac{M(x_1)}{C(x_1)} - y_j\right] \tag{36}$$

in which w_i are weighting factors for numerical integration. The estimates are then checked by calculating new values of T_s and M_s from Equations 14 and 17, respectively, based on an assumed uniaxial stress-strain relationship for the longitudinal steel. In case of error, the analysis is repeated with revised estimates of the structural variables T_s and M_s until the calculated values converge to estimated values within an allowable tolerance. This tolerance was specified in the range of 0.5 to 1.0 % in this study.

Numerical Formulation for Solution of Sectional Response Variables

For a section i discretized into N_f number of fibers along the length of the wall (in the *y* direction), the fiber stresses can be numerically integrated to obtain the internal masonry forces $C(x_i)$ and $V(x_i)$ and masonry moment $M(x_i)$ using Equations 13, 15 and 16 as follows:

$$C(x_i) = \sum_{k=1}^{N_f} w_k \cdot \sigma_x(x_i, y_k)\cdot b \cdot t_k \tag{37}$$

$$V(x_i) + V_s(x_i) = \sum_{k=1}^{N_f} w_k \cdot \tau_{xy}(x_i, y_k)\cdot b \cdot t_k \tag{38}$$

$$M(x_i) = \sum_{k=1}^{N_f} w_k \cdot y_k \cdot \sigma_x(x_i, y_k)\cdot b \cdot t_k \tag{39}$$

in which the subscript *k* refers to the k^{th} fiber. Thus, y_k is the *y* coordinate of the fiber midpoint, t_k the thickness, w_k the weighting factor of k^{th} fiber for numerical integration, $\sigma_x(x_i, y_k)$ is the average normal stress in the k^{th} fiber and $\tau_{xy}(x_i, y_k)$ is the average shear stress on the face of k^{th} fiber in the i^{th} section [Figure 2(g)].

From assumption 1 (or Equation 12) and assumption 2 (or Equation 18), the normal stress $\sigma_x(x_i, y_k)$ in the fiber is a function of the strain variables $\xi(x_i)$ and $\Phi(x_1)$ and shear stress $\tau_{xy}(x_i, y_k)$. In mathematical terms,

$$\sigma_x(x_i, y_k) = \sigma_x\left[\{\xi(x_i) + y_k \cdot \Phi(x_i)\}, \tau_{xy}(x_i, y_k)\right] \quad \textbf{(40)}$$

Substituting into Equations 37 and 39,

$$C\left[\xi(x_i), \Phi(x_i), \tilde{\tau}_{xy}(x_i)\right] = \sum_{k=1}^{N_f} w_k \cdot \sigma_x \begin{bmatrix} \{\xi(x_i) + y_k \cdot \Phi(x_i)\}, \\ \tau_{xy}(x_i, y_k) \end{bmatrix} \cdot b \cdot t_k \quad \textbf{(41)}$$

$$M\left[\xi(x_i), \Phi(x_i), \tilde{\tau}_{xy}(x_i)\right] = \sum_{k=1}^{N_f} w_k \cdot y_k \cdot \sigma_x \begin{bmatrix} \{\xi(x_i) + y_k \cdot \Phi(x_i)\}, \\ \tau_{xy}(x_i, y_k) \end{bmatrix} \cdot b \cdot t_k \quad \textbf{(42)}$$

where the symbol $\tilde{\tau}_{xy}(x_i)$ denotes the shear stress distribution at the i^{th} section.

Since masonry exhibits a nonlinear stress-strain relationship, the internal masonry force $C(x_i)$ and moment $M(x_i)$ are nonlinear functions (equations 41 and 42) of the strain variables $\xi(x_i)$ and $\Phi(x_i)$. However, given the values of the structural force T_s and moment M_s due to longitudinal reinforcing steel, the internal masonry force $C(x_i)$ and moment $M(x_i)$ are uniquely defined for any section i using section equilibrium equations 33 and 34. Therefore, for the estimated values of steel force T_s and moment M_s , the masonry force $C(x_i)$ and moment $M(x_i)$ are defined for the i^{th} section, and the unknown masonry strain variables $\xi(x_i)$ and $\Phi(x_i)$ can be obtained by using a suitable numerical method to solve the simultaneous nonlinear Equations 41 and 42 for an assumed shear stress distribution $\tilde{\tau}_{xy}(x_i)^a$. Detailed methodology and flowcharts of the numerical solution using a Newton-Raphson procedure may be found elsewhere [Madan, Reinhorn et al. (1996)]. The solution of the masonry strain variables $\xi(x_i)$ and $\Phi(x_i)$ completely determines the stress and strain conditions in all the masonry fibers at the section for the assumed shear stress distribution $\tilde{\tau}_{xy}(x_i)^a$ (Assumptions 1 and 2), therefore, stress and strain distributions along the section length are provided.

The correct shear stress distribution at section *i* for the given structural force T_s and moment M_s (due to longitudinal reinforcing steel) is obtained using the dual section analysis proposed by Vecchio and Collins (1988). A conjugate section at an infinitesimally small distance δx away is considered. For the sake of clarity, the discrete section *i* will be denoted as section *i1* and the conjugate section will be referred to as section *i2* [Figure 3 (d)]. The masonry stress and strain distributions are calculated at the conjugate section *i2* in the same manner (outlined in the previous paragraph) as for section *i1* (i.e. section i), assuming the shear stress distribution to be identical to that at section *i1* (Assumption 3), i.e.,

$$\tilde{\tau}_{xy}(x_{i1}) = \tilde{\tau}_{xy}(x_{i2}) = \tilde{\tau}_{xy}(x_i)^a \quad \textbf{(43)}$$

A new estimate of the shear stress distribution $\tilde{\tau}_{xy}(x_i)^c$ is then computed by considering the longitudinal equilibrium of the elements or fibers bounded by the conjugate sections using equilibrium Equation 20 [Figure 3(d)]. The shear stress intensity is computed at a defined number of nodes n_n along the section depth [Figure 2(h)] using Equation 20. The horizontal shear stress $\tau_{xy}(x_i, y_n)$ acting on the n^{th} node is calculated from the longitudinal equilibrium Equation 20 [Figure 3(d)] using the normal stress distributions obtained for the conjugate sections as outlined in the previous paragraph. The numerical formulation for the solution of the longitudinal equilibrium equation (Equation 20) is presented by Vecchio and Collins (1988) and Madan (1996). The new shear stress distribution $\tilde{\tau}_{xy}(x_i)^c$, thus computed by solving Equation 20, is compared with the assumed distribution $\tilde{\tau}_{xy}(x_i)^a$ at the location of each node [Figure 5]. If the comparison does not satisfy a defined convergence criteria, the assumed shear stress distribution is revised and the analysis repeated for the section. The shear stress distribution is thus iterated until the convergence criteria is satisfied by the assumed and computed shear stress distributions. The shear stress distribution assumed for any iteration is a corrected estimate based on a weighted average of the assumed and computed distributions of the previous iteration [Figure 5].

Algorithm for Numerical Analysis

Based on the foregoing numerical modeling and formulation, an incremental iterative algorithm was developed for analyzing the inelastic lateral force-displacement response of concrete masonry shear walls with unbonded reinforcement. The solution procedure functions by displacement control effected by incrementing curvature at the base of the wall $\Phi(x_1)$. A flowchart of the numerical solution algorithm is presented in Figure 5. The procedure begins by assuming the unknown structural quantities T_s and M_s for a control curvature $\Phi(x_1)$ at the base section (i = 1). The solution algorithm computes the unknown masonry strain $\xi(x_1)$ at the base section for the assumed value of the structural variable T_s using sectional force equilibrium Equations 33 and 41. The algorithm proceeds to compute the external moment $M_z(x_1)$ at the base section using sectional moment equilibrium Equations 34 and 42, which in turn determine the external moments $M_z(x_i)$ at higher sections by static equilibrium of the sections. The solution procedure then computes the sectional masonry strain variables $\xi(x_i)$ and $\Phi(x_i)$ at each of the finite sections (i = 2, N_s) above the base by using sectional equilibrium Equations 33, 34, 41, 42. The shear stress distribution at each section is determined using the dual section analysis technique described in the foregoing paragraph. Subsequent to de-

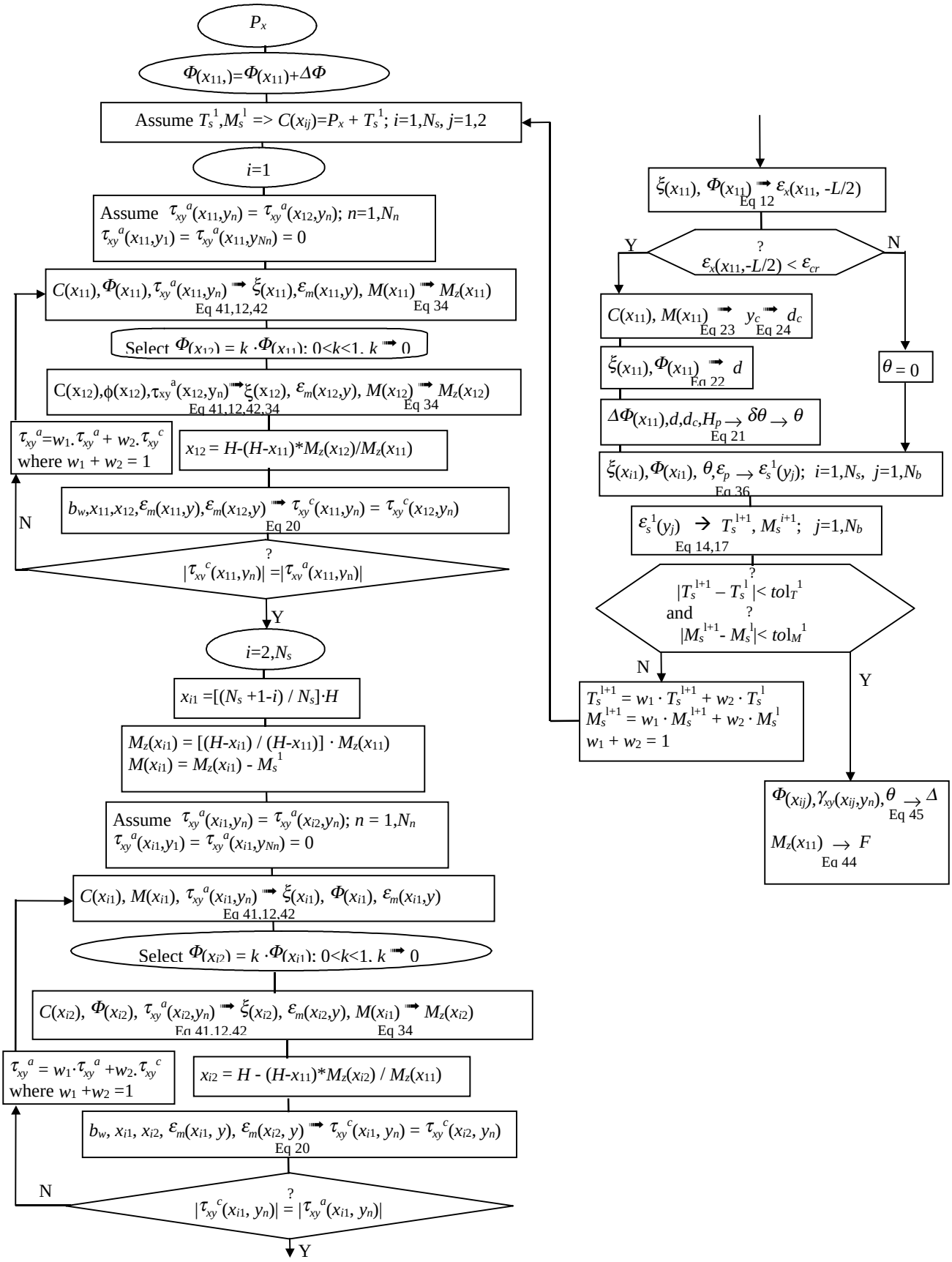

Figure 5—Flowchart of Numerical Solution Algorithm

termination of the masonry strain profiles $\varepsilon_x(x_i, y)$ and shear stress distributions $\tau_x(x_i, y)$ at all the discrete sections, the algorithm checks for the existence of uplift or rigid body motion. Uplift is assumed to initiate with the onset of cracking at the windward edge of the base. The uplift angle, θ, was computed using Equations 21 to 24. Thereafter, strains $\varepsilon_s(y_j)$ in vertical unbonded rebars are computed using Equation 36, which further provide the steel force T_s and moment M_s using Equations 14 and 17, respectively. The computed steel force and moment are compared with the assumed values to check if the errors are greater than the specified tolerances. If so, the steel force T_s and moment M_s are revised and the entire analysis is repeated for the control curvature $\phi(x_1)$. The steel force and moment are iterated until convergence is achieved. After force and moment convergence is achieved, the algorithm computes the lateral in-plane force, F, corresponding to the control curvature $\phi(x_1)$ at the base section using the static equilibrium of the wall as follows:

$$F = V_y(x_0) = \frac{M_z(x_0)}{(H - x_0)} \tag{44}$$

in which the subscript o refers to any arbitrary section.

The lateral in-plane displacement (Δ) at the wall top is computed from Equation 32 using numerical integration as follows:

$$\begin{aligned}\Delta = v(x_{Ns}, y_{Nf}) = \\ \sum_{i=1}^{N_s}\sum_{k=1}^{N_f} w_i\, \gamma_{xy}(x_i, y_k)\cdot \Delta x_i + \\ \sum_{i=1}^{N_s} w_i' \cdot \Phi(x_i)\cdot (h - x_i)\cdot \Delta x_i + \theta \cdot H\end{aligned} \tag{45}$$

in which w_i and w_i' are weighting actors for numerical integration.

Numerical Analysis Procedure for the Special Case of Bonded Reinforcement

The proposed numerical analysis procedure can be applied with some modifications for analysis of masonry shear walls with grouted (bonded) longitudinal reinforcement as well. Because of bonding, however, the steel force T_s and moment M_s vary from one cross-section to another and are therefore calculated at the i^{th} section as:

$$T_s(x_i) = \sum_{j=1}^{N_b} E_s(\varepsilon_s)\cdot A_{sj}\cdot \varepsilon_s(x_i, y_j) \tag{46}$$

$$M_s(x_i) = \sum_{j=1}^{N_b} y_j \cdot E_s(\varepsilon_s)\cdot A_{sj}\cdot \varepsilon_s(x_i, y_j) \tag{47}$$

Strains $\varepsilon_s(x_i, y_j)$ in the longitudinal reinforcing bars at any section i are directly related to the sectional masonry strain variables $\xi(x_i)$ and $\Phi(x_i)$ using compatibility Equation 9 and assumption 1 [Equation 12] as follows:

$$\begin{aligned}\varepsilon_s(x_i, y_j) = \varepsilon_p + \varepsilon_x(x_i, y_j) = \\ \varepsilon_p + \left[\xi(x_i) + y_j \cdot \Phi(x_i)\right]\end{aligned} \tag{48}$$

This compatibility condition needs to be considered instead of Equation 28 when computing strains in the bonded reinforcing bars at any section. Further, the steel force T_s and moment M_s need to be calculated and iterated at each section to obtain the independent response of that section. In addition, the contribution of dowel action provided by the longitudinal reinforcement also needs to be considered when calculating the shear stress distribution at any section. This would imply using Equation 19 instead of Equation 20. Further, in case of bonded reinforcement, the rigid body rotation θ due to uplift should be set to zero by setting the value of the parameter H_p in Equation 21 to be zero. The modifications required in material properties have been noted previously.

ANALYSIS

The numerical procedure described in the preceding part of the paper was implemented to analyze the lateral in-plane force-displacement characteristics of the reinforced masonry shear wall model shown in Figure 2. The vertical (longitudinal) reinforcing bars are unbonded and anchored into rigid beams at the top and bottom ends of the wall. The bottom beam is fixed to the ground and a concentrated lateral load is applied to the top beam. For numerical analysis, the shear wall model was discretized into 5 sections along the height. The shear wall was modeled as a cantilever (fixed at the base and free at the top) for calculating external bending moments and shear forces acting on the discrete sections. The numerical integration of masonry stresses was performed by subdividing each discrete section into a finite number of fibers along the wall length. A parabolic variation of normal stress was assumed within the fiber element for numerical integration. An adaptive subdivision scheme was used to arrive at the optimum number and thickness of fibers based on the non-linearity of stress distribution over the wall length. The scheme proposed by Collins et al. (1990) for fiber element modeling of a reinforced concrete section enables self-generation of fiber elements over the section by automatically refining the fiber size in regions with high stress gradients. The iterative solution of the sectional masonry strain variables $\xi(x_i)$ and $\Phi(x_i)$ was obtained using the Newton-Raphson method. Shear stresses were computed at 100 uniformly spaced nodes along the section depth [Figure 2(h)] using Equation 20. Numerical integration in Equations 36 and 45 was performed using Simpson's rule. The crushing strain of masonry was assumed to be 1.5% based on typical stress-strain curves obtained from

compression testing of concrete masonry prisms [Englekirk and Hart (1984)], which show that the material can sustain stress until strains as high as 2% prior to failure due to crushing. Past research data indicated that the cracking stress, f_{cr}, of masonry typically ranges from 5% to 15% of the masonry prism strength, f'_m, (peak compressive stress). A conservative value of cracking stress, equal to 5% of the masonry prism strength, was adopted for the numerical analysis.

EXPERIMENTAL VERIFICATION

An experimental study was performed at the State University of New York at Buffalo to evaluate the seismic performance of concrete masonry shear walls with unbonded vertical reinforcement [Madan (1996)]. Six wall specimens were tested under in-plane lateral loading in displacement control to investigate the influence of various parameters including axial loading, wall aspect ratio, loading method (monotonic or cyclic), prestress in longitudinal reinforcement, and reinforcement anchorage and splicing, on the in-plane lateral load behavior of such walls. Experimental data obtained from the testing was used to verify the proposed model by comparing the observed response with that predicted using the model. For the sake of brevity, results of comparison for only two wall specimens (test specimens 2 and 6) are presented herein. The first test specimen (Specimen 2) was designed to exhibit a predominantly flexural mode of failure (flexure-critical), and the second wall specimen (Specimen 6) was designed for a dominant shear failure mode (shear-critical). During the tests, each specimen was first subjected to in-plane lateral quasi-static cyclic loading under a constant axial load of 31 kN (6,970 lb) followed by cyclic loading under a constant 115 kN (25,852 lb) axial load. The unbonded vertical reinforcing bars in test Specimen 6 were prestressed. The typical configuration of the two test specimens is illustrated in Figure 6. The figure also displays the important test parameters for Specimens 2 and 6. In order to ensure shear transfer at the top beam-wall interface, the uppermost course in the wall is constructed with grouted bond beam units. The top beam is connected to the wall through a steel plate with shear key projections that are embedded in the grout. The in-plane horizontal (lateral) and vertical (axial) loads were applied using servo-controlled hydraulic actuators, each equipped with an in-series load cell to measure the loads. The test specimens were also instrumented with several sonic displacement transducers and linear potentiometers to measure the absolute as well as relative displacements. Details of the test setup, instrumentation and methodology are presented by Madan, 1996.

Extensive data were measured and collected during the experimental program that involved testing of six wall specimens under in-plane cyclic loading. Analysis of the displacement data established that the average height of the stressed zone, H_p, at the extreme compression fiber (above the toe) in flexure-critical wall specimens generally varies from 0.1H to 0.4H for a practical range of axial loads and wall aspect ratios [Madan (1996)]. Further, the height of the stressed zone, H_p, is approximately proportional to the magnitude of the axial load. For shear-critical test specimens, on the other hand, the average height of the stressed zone, H_p, above the wall toe was found to be negligible. The observation is reasonable since the shear-critical wall specimens did not undergo uplift during testing due to their small aspect ratio. For the purpose of numerical analysis, the value of height, H_p, in flexure-critical test Specimen 2 was $0.1H$, in the case of 31 kN (6,970 lb) axial load, and $0.4H$, in the case of 116 kN (26,080 lb) axial load. For numerical analysis of shear-critical Specimen 6, the height, H_p, was specified as zero in order to eliminate the uplift component of the response. The prism strength of masonry was scaled down for analyzing the in-plane response under 116 kN (26,080 lb) axial load in order to account for strength degradation due to prior cycling of the test specimens under 31 kN (6,970 lb) axial load. The reduction factors for scaling were estimated from the strength deterioration observed in the test specimens at the end of testing under 31 kN (6,970 lb) axial load.

The observed hysteretic load-displacement curves obtained from quasi-static cyclic testing of the flexure-critical wall Specimen 2 under axial loads of 31 kN (6,970 lb) and 116 kN (26,080 lb) are shown in Figures 7 (a) and (b) respectively. The salient parameters of the test are also included in the figure. The monotonic load-displacement relationships predicted by the proposed model are superimposed on the experimental hysteresis loops for each case. Figures 7 (c) and (d) show similar comparisons of experimental vs. theoretical load-displacement relationships for the shear-critical test Specimen 6 under axial loads of 31 kN (6,970 lb)and 116 kN (26,080 lb), respectively. Comparisons of the experimentally measured force-displacement curves and theoretically estimated envelopes demonstrate that the proposed analysis procedure, in general, predicts the in-plane lateral force-displacement envelope of the tested shear wall specimens with a fair degree of accuracy. Minor deviations in the analytically predicted behavior from experimentally observed response may be explained in terms of variation in material properties and limitations of the underlying assumptions of the model. One such assumption is that plane sections remain plane, which may not be valid in the disturbed end regions. The abrupt descent of the theoretically obtained lateral load-deformation envelope for test Specimen 2 under 116 kN (26,080 lb) axial load signifies crushing of masonry at the extreme compression fiber at the wall base (i.e. the toe of the wall), which causes a sharp decline in the lateral strength of the wall at 32 mm (1.25 in.) lateral displacement. Since the envelope of experimentally measured curves does not display such a transition, it may be argued that the crushing strain was underestimated in theory. Further, the analytical model is developed for mono-

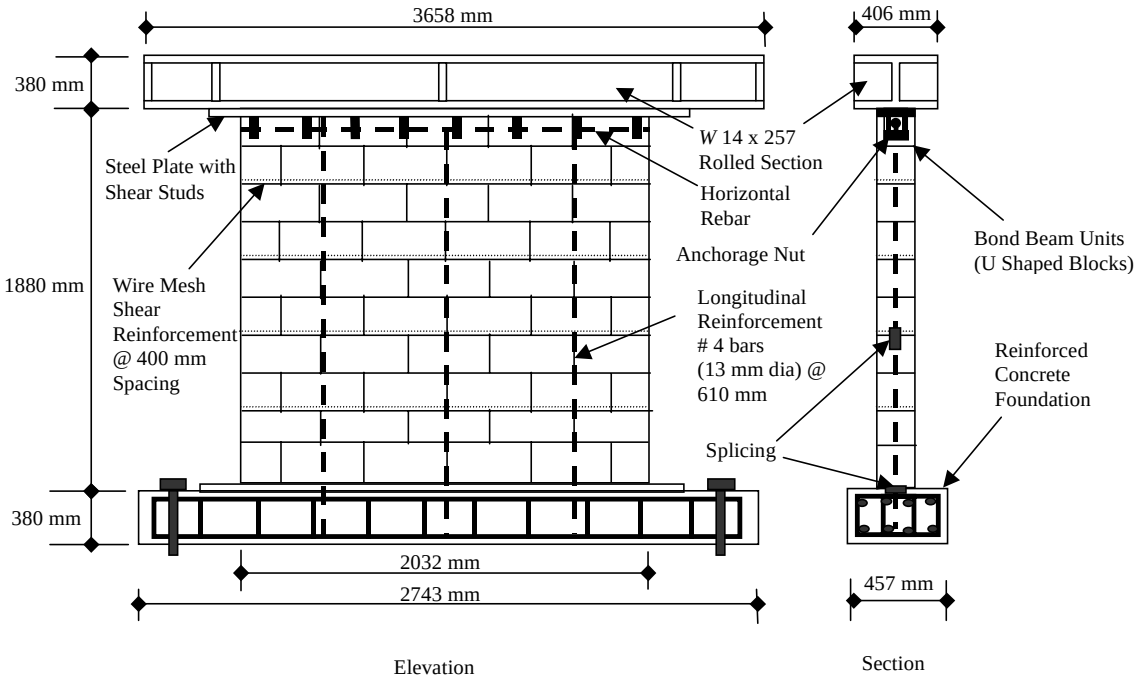

Specimen No.	Test No.	Axial Load (kN)	Effective Wall Height (mm)	Vertical Reinforcement (mm^2/ mm)	Shear Reinforcement (A_h / s_h) (kN)	Pretensioning Force Mode	Dominant Failure	Loading History
2	1	31	2286	0.026	1.219 / 406	0.00	Flexure	Sinusoidal Drift History @ 0.1 and 0.2 Hz
	2	116	2286	0.026	1.219 / 406	0.00	Flexure	
6	1	31	1016	0.029	1.219 / 203	59.97	Shear	Sinusoidal Drift History @ 0.1 and 0.01 Hz
	2	116	1016	0.029	1.219 / 203	0.00	Shear	

Figure 6—Test Wall Specimen 2: Typical Details (1 mm = 0.039 in., 1 kN = 224.8 lb)

tonic loading and, thus, does not account for strength and stiffness degradation under repeated load reversals. Hence, analytical predictions of the lateral strength and stiffness of wall specimens under 116 kN (26,080 lb) axial load may diverge from experimental results due to error in estimating degraded masonry strength and stiffness after cycling under 36 kN (8,093 lb) axial load.

Figure 8 presents a typical illustration of the spatial variation in elemental stress conditions over the wall surface. That figure illustrates the distributions of principal compressive stress, shear stress, and angle of inclination of principal compressive stress (each plotted along the wall length) at the base, mid-height and top sections of wall Specimen 2 under 31 kN (6,970 lb) axial load. A qualitative study of the figure reveals that the intensity of principal compressive stress distribution at the top section of the wall is greatest at the loaded end and decreases along the wall length. On the other hand, the intensity of compressive stress distribution at the base section is maximum at some point near the toe and decreases towards the heel of the wall. In fact, the principal stresses at the base section enter into the tensile range within a very short span of length away from the wall toe, thus indicating a concentrated compression in the contact region near the toe and a loss of contact (or uplift) at the heel. The foregoing observations suggest that the compression field in the masonry wall follows an inclined trajectory from the loaded end of the wall to the compressed contact region at the toe. The results of stress distribution provided by the analysis can be used to calculate the exact direction and magnitude of the compressive stress resultant (masonry compression strut) across the masonry wall.

DESIGN CONSIDERATIONS

Application of the proposed micro-element model (micro-model) is tedious and time-consuming. Because of the substantial computational effort required, it may not be cost-effective to implement the model for routine design of masonry shear walls with unbonded reinforcement. For design purposes, it is more efficient to use the flexure model presented by Madan, Reinhorn et al. (1996) to evaluate in-plane flexural strength and ductility of the wall. However, since the flexure model inherently neglects shear behavior, design based on the model needs to be complemented with a methodology for assessing safety of the wall against shear failure. Current code provisions for masonry design account for the interaction of shear and flexure using overly

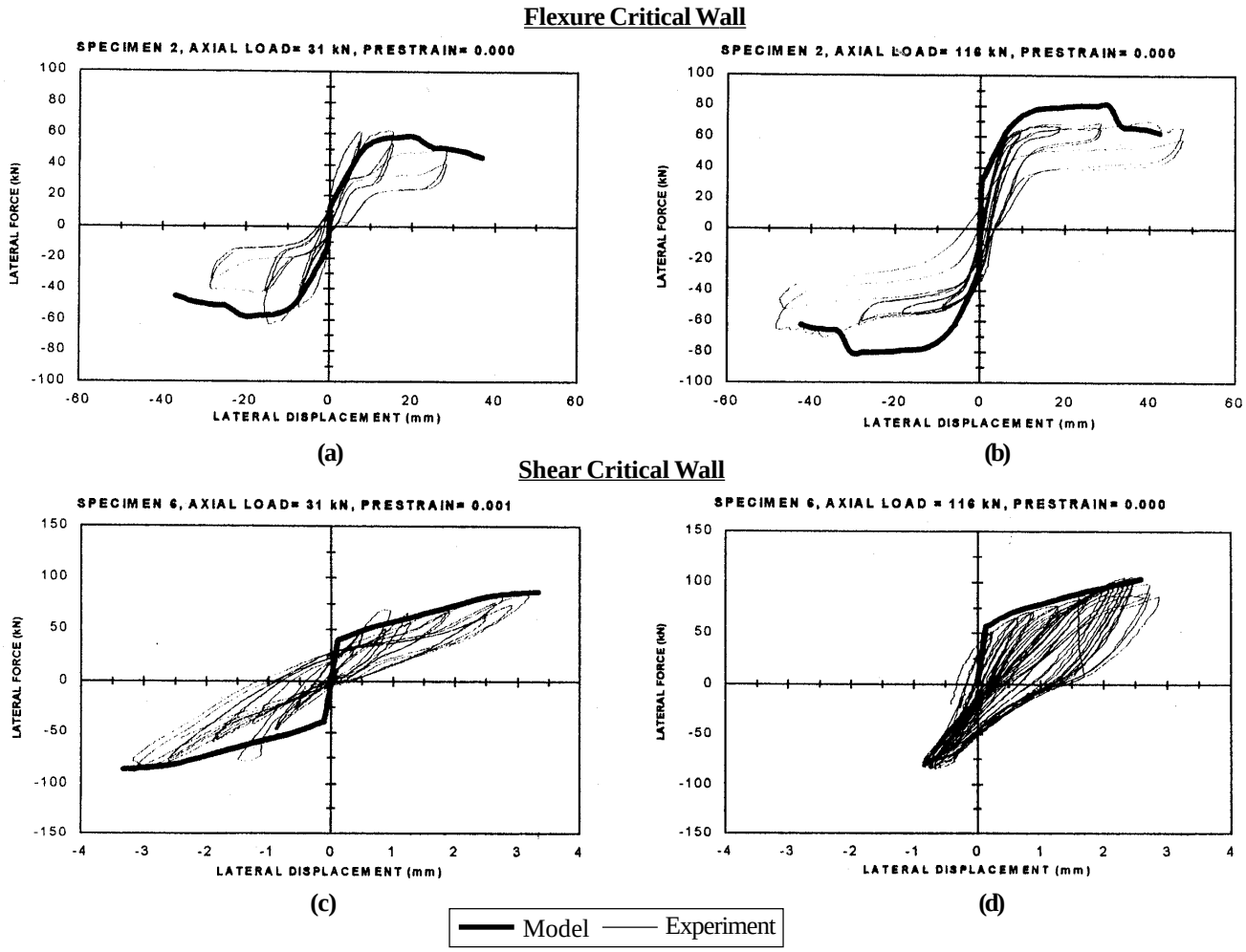

Figure 7—Theoretical vs. Experimental In-Plane Force Displacement Response for (a) Test Specimen 2 under 31 kN axial load, (b) Test Specimen 2 under 116 kN axial load, (c) Test Specimen 6 under 31 kN axial load, (d) Test Specimen 6 under 116 kN axial load (1 mm = 0.039 in., 1kN = 224.8 lb)

simplified semi-empirical equations, which may be unduly conservative or inaccurate for the purpose of inelastic design. Vecchio and Collins (1988) have presented interaction curves for inelastic analysis of concrete sections under combined shear and moment. However, there remains a need for rational guidelines to account for interaction of shear and flexure in strength or inelastic design of masonry.

In masonry shear walls with unbonded vertical reinforcement, the component of shear stress due to dowel action of the longitudinal reinforcement (i.e., the second term in Equation 19) is zero, so no shear force is resisted by the longitudinal rebars, i. e., $V_s(x_i) = 0$ at any section i. Thus, Equation 3 reduces to

$$V_y(x_i) = V(x_i) \quad \textbf{(49)}$$

The critical section for shear failure in masonry shear walls with unbonded vertical reinforcement under in-plane lateral load is at the base. From Equation 49, the shear capacity of the base section is essentially the shear capacity, V^u, of masonry in contact with the foundation, which depends on the moment M and axial force C in the masonry.

A parametric study was performed to study interaction of the shear force V^u and moment M^u in monotonically loaded masonry at the ultimate limit state for varying values of axial force C. Results of the study are summarized by the interaction curves plotted in Figure 9. The curves shown in the figure employ dimensionless parameters to depict the interaction of shear force and bending moment in concrete masonry sections at the ultimate limit state for different magnitudes of axial force. Therefore, these curves can be universally applied for evaluating the shear and flexural capacity of concrete masonry subjected to combined shear and flexure. The figure illustrates that, in general, failure is governed by flexure for aspect ratios (M / Vd) greater than 1.0. For aspect ratios smaller than 1.0, failure depends on the level of axial force – the higher the axial force, the more prone the member is to shear failure. The interaction curves presented in Figure 9 can be adopted for strength design of unreinforced masonry or even masonry with unbonded steel reinforcement.

In this paper, an integrated design methodology is proposed for masonry shear walls with unbonded reinforce-

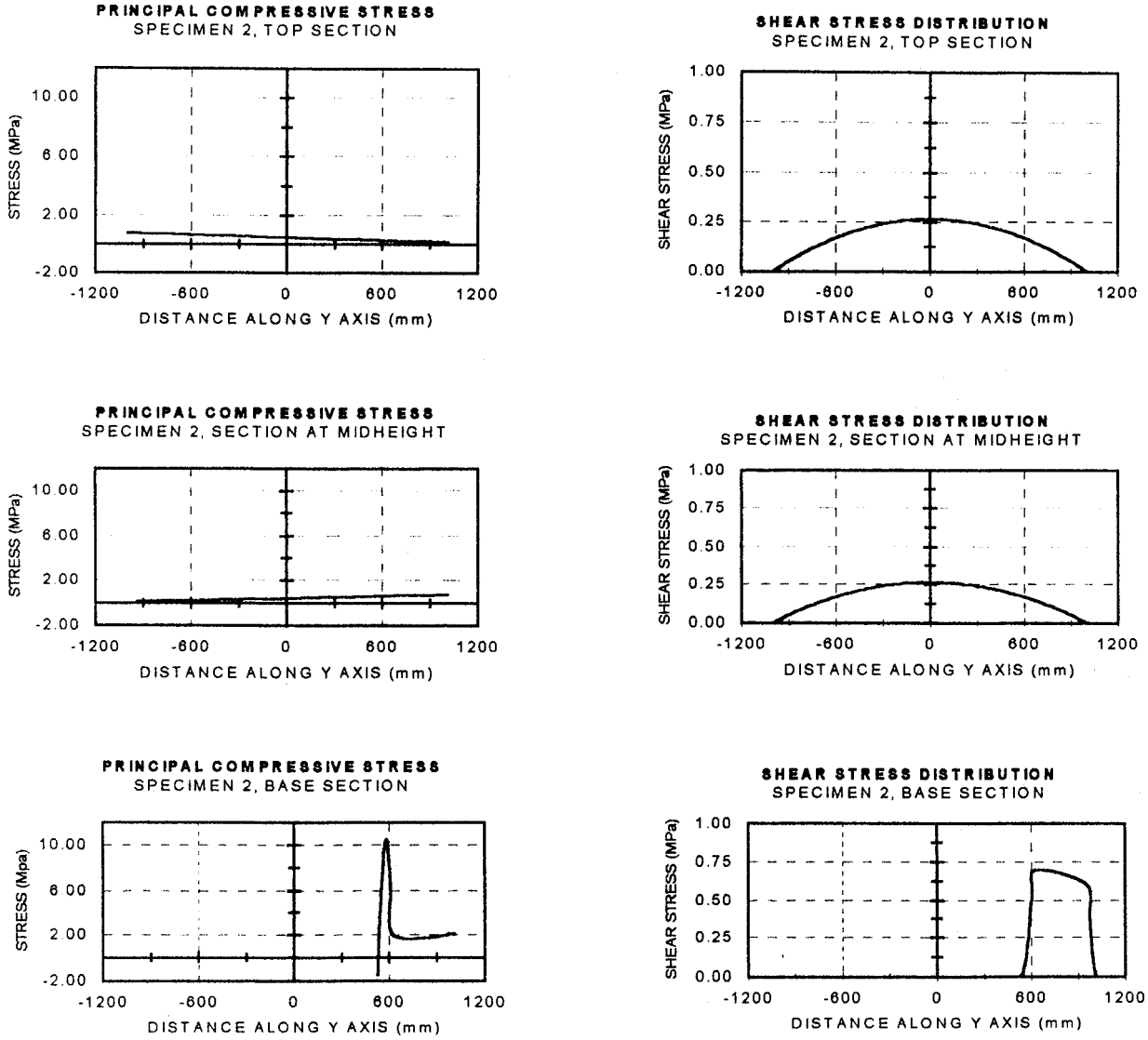

Figure 8—Spatial Variation of Stress Conditions in Test Specimen 2 under 31 kN Axial Load (1 mm = 0.039 in., 1kN = 224.8 lb, 1MPa = 145 psi)

ment. The methodology involves implementation of the flexure model proposed earlier by the authors [Madan, Reinhorn and Mander (1996)] in conjunction with the interaction curves presented in Figure 9. The authors recommend that flexure model be used for evaluating the flexural strength and ductility of the masonry shear wall. The ultimate moment, M^u, in masonry at the base obtained from results of flexural response analysis can be subsequently used to estimate the shear force capacity, V^u, of masonry at the base by using the shear - moment capacity interaction curves presented in Figure 9. Since the shear strength of the wall equals the shear force capacity of masonry at the base, the wall can be designed to resist shear failure by ensuring that the external shear force does not exceed the estimated shear force capacity of masonry at the base, i.e., $V_y < V^u$.

CONCLUSIONS

The fiber element (micro-element) model presented in this paper provides a unified analytical approach for evaluating the in-plane lateral force-displacement envelope of masonry shear walls with unbonded vertical reinforcement by taking into account the interaction of flexure, shear and uplift. The model enables detailed nonlinear analyses of such walls by furnishing a complete solution of the force and displacement as well as stress and strain fields in the wall using rational considerations of force equilibrium and displacement compatibility. The model permits the use of realistic constitutive models for component materials and treats the various governing factors in a general manner. Further, the modeling approach is versatile, in that the analytical formulation of the model can be readily modified to

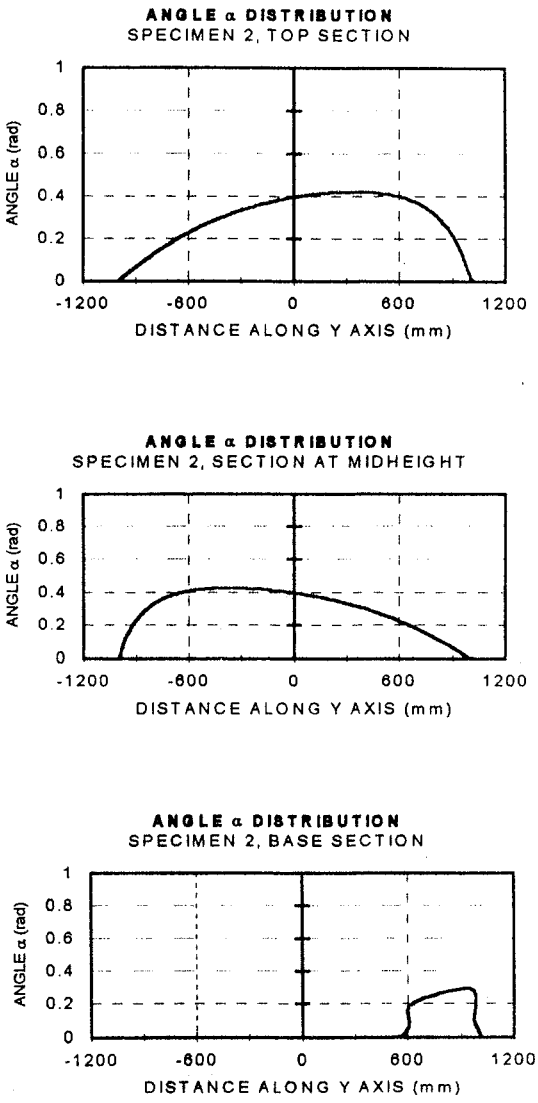

Figure 8—continued

account for different boundary conditions and loading patterns. The proposed micro-model provides a powerful research tool and may be effectively implemented in situations that warrant such a meticulous analysis. For purposes of design, the proposed analytical technique was applied to a parametric study to generate interaction curves that can be conveniently used for evaluating the shear resistance of concrete masonry sections subjected to combined shear and bending. The interaction curves, in conjunction with the flexure model proposed by the authors in an earlier paper [Madan, Reinhorn and Mander (1996)] provide an integrated design methodology for masonry shear walls with unbonded longitudinal reinforcement, taking into account interaction of shear and flexure under in-plane lateral loading.

REFERENCES

Collins, M. P. and Mitchell, D., "Prestressed Concrete Structures," Prentice Hall, New Jersey, 1990.

Englekirk, R. E., Hart, G. C. and The Concrete Masonry Association of California and Nevada, " Earthquake Design of Concrete Masonry Buildings: Volume 2 - Strength Design of One- to Four- Story Buildings," Prentice Hall, Englewood Cliffs, NJ 07632, 1984.

Hart, G. C., "Seismic Design of Ductile Masonry Walls," The Masonry Society Journal, The Professional Journal of the Masonry Society of America, pp. 24-35, 1991.

Madan, A., " Non-Linear Modeling of Masonry Walls for Planar Analysis of Structures," Ph. D Dissertation, Department of Civil Engineering, State University of New York, Buffalo, NY, March 1996.

Madan, A., Reinhorn, A. M. and Mander, J. B., "Analysis of Concrete Masonry Shear Walls with Unbonded Reinforcement under Reversed Cyclic Loading," Proceedings of the 5th Australasian Masonry Conference, Gladstone, Queensland, Australia, July 1 – 3, 1998, pp. 243 – 254.

Madan, A., Reinhorn, A. M. and Mander, J. B., "Flexural Behavior of Reinforced Masonry Shear Walls with Unbonded Reinforcement," The Masonry Society Journal, The Professional Journal of the Masonry Society of America, Vol. 14, No. 1, pp 87 - 98, August 1996.

Mander, J. B., Priestley, M. J. N. and Park, R., " Theoretical Stress-Strain Behavior of Confined Concrete," Journal of Structures Division, ASCE, Vol. 114, No. 8, pp. 1827-1849, Aug 1988.

Park, R. and T. Paulay, "Reinforced Concrete Structures," John Wiley & Sons, New York, 1975.

Priestley, M. J. N., Seismic Assessment of Existing Concrete Bridges," University of California, San Diego, Structural Systems Research Report, Report No. SSRP 91/03.

Shing, P. B., Noland, J. L., Klamerus, E. and Spaeh, H., "Inelastic Behavior of Concrete Masonry Shear Walls", Journal of Structural Engineering, ASCE, 115 (9), pp. 2204-2225, 1989.

Vecchio, F. J. and Collins, M. P., " Predicting the Response of Reinforced Concrete Beams Subjected to Shear Using Modified Compression Field Theory," Technical Paper, ACI Structural Journal, pp. 258-268, May-Jun 1988.

SHEAR-MOMENT INTERACTION CURVES FOR MASONRY WALLS AT ULTIMATE LIMIT STATE UNDER MONOTONIC IN-PLANE LATERAL LOADING FOR GIVEN AXIAL LOAD C

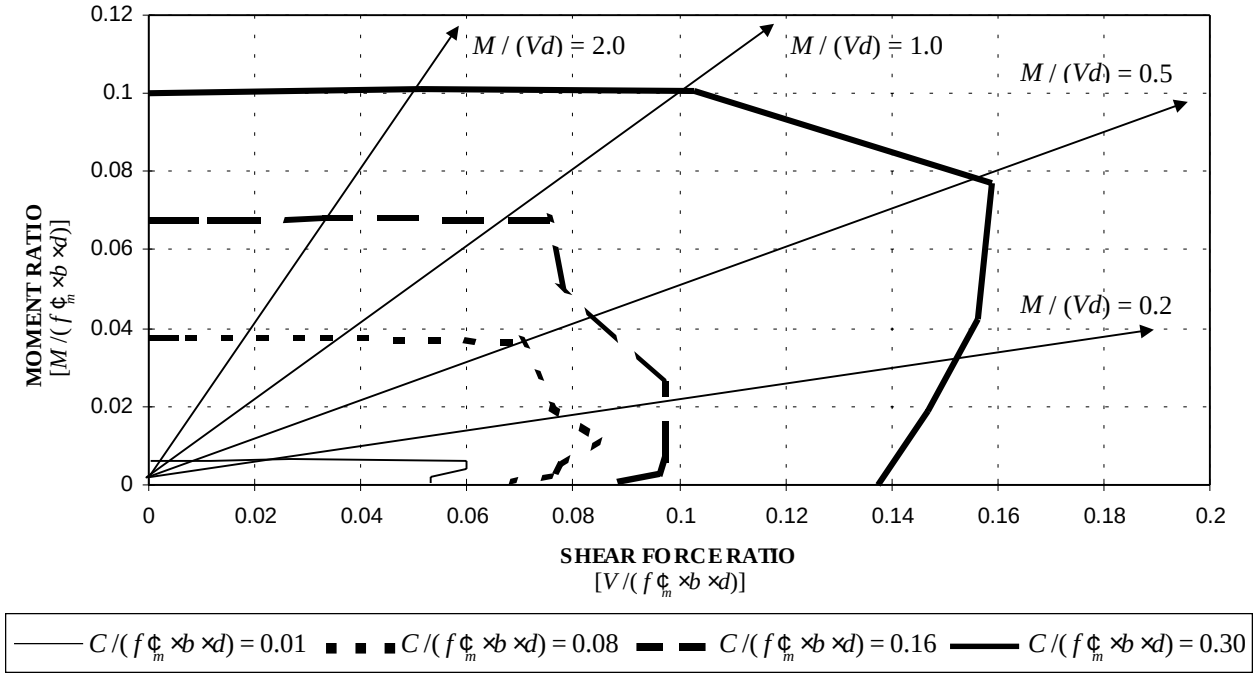

Figure 9—Dimensionless Shear Moment Capacity Interaction Curves for Shear Design of Masonry Walls with Unbonded Reinforcement

NOTATIONS

A_h = horizontal steel reinforcement of area.
A_{sj} = cross sectional areas.
b = width.
b_w = equals wall width b.
C = point of reaction.
$C(x_i)$ = internal compressive forces in masonry.
d = contact length.
d_c = distance.
dx = small distance.
E_m = initial slope of the stress-strain curve.
E_s^0 = modulus of elasticity.
E_{sec} = slope of the secant to the peak stress.
f_{cr} = cracking strain.
f_m = stress.
$f\,¢_m$ = peak compressive stress.
f_{mt} = tensile stress.
f_s = steel stress.
f_y = yield strength of steel.
F = lateral in-plane force.
H = height.
H_p = average height of the compressed zone.
j = refers to the j^{th} bar.
k = refers to the k^{th} fiber.
L = length.
$M(x_i)$ = internal resisting moments due to masonry.
M_s = unknown structural moment.
$M_s(x_i)$ = internal resisting moments due to steel.
M_z = in plane bending movement.
M^u = ultimate moment.
N_b = unbonded vertical rebars.
N_f = number of fibers along the length of the wall (in the y direction).
N_s = finite number of sections.
P_x = vertical axial force.
t_k = the thickness.
T_s = unknown structural force.
$T_s(x_i)$ = internal tensile forces in steel.
$u(x_i, y)$ = vertical displacement in the longitudinal x direction at coordinates (x, y)
$u_r(x_i, y)$ = the vertical in-plane displacement due to rigid body uplift.
$u_s(x_i, y)$ = the vertical (longitudinal) in-plane displacement due to strain deformations of the wall.
$v(x_i, y)$ = total lateral in-plane displacement.
$v_r(x_i, y)$ = uplift-produced lateral in-plane displacement.
$v_s(x_i, y)$ = strain deformation-produced lateral in-plane displacement.
$V(x_i)$ = internal shear force in the horizontal y direction due to masonry's shear resistance.

$V_s(x_i, y)$ = shear resistance of masonry in the y direction due to dowel action of longitudinal steel.
V_y = lateral shear force.
V^u = shear force capacity.
w_i = weighting factors for numerical integration.
w_i¢ = weighting factors for numerical integration.
w_k = weighting factor of the k^{th} fiber.
W = wall weight.
x = coordinate.
y = coordinate.
y_c = y coordinate of point of action.
y_j = j^{th} rebar at the y coordinate.
y_k = y coordinate of the fiber midpoint.
a_1 = factor accounting for bond characteristics of the steel reinforcement.
a_2 = factor depending on the nature of loading.
dx = conjugate section at an infinitesimally small distance.
D = lateral displacement.
e_{cr} = cracking strain.
$e_h(x_i, y)$ = horizontal steel strain in the i^{th} section at coordinate y.
e_m = strain.
e¢$_m$ = peak compressive strain.
e_{mt} = tensile strain.
e_p = strain in the masonry resulting from the applied vertical prestress in the rebar.
e_s = steel strain.
$e_s(y_j)$ = uniaxial longitudinal strain.
$e_s(x_i, y_j)$ = strain in the vertical rebar j at any cross-section i.
$e_x(x_i, y)$ = distribution of normal strain.
e_y = normal strain in the masonry in the y direction.
$F(x_i)$ = angle of inclination of the linear strain profile or the flexural curvature at the i^{th} section.
s_h = horizontal steel stress in the i^{th} section at coordinate y.
$s_x(x_i, y)$ = normal stress in a masonry element at coordinate y in the i^{th} section.
$s_x(x_i, y_k)$ = normal stress in the fiber.
s_y = normal stress in masonry in the y direction.
q = rigid body rotation.
$t_{xy}(x, y)$ = shear stress distribution.
$\tilde{\tau}_{xy}(x_i)$ = shear stress distribution of the i^{th} section.
$t_{xy}(x_i)^a$ = assumed shear stress distribution.
$t_{xy}(x_i)^c$ = estimate of the shear stress distribution.
$t_{xy}(x_i, y)$ = shear stress distribution.
$t_{xy}(x_i, y_k)$ = average shear stress on the face of k^{th} fiber in the i^{th} section.
$x(x_i)$ = masonry strain variable.
¶d_c = incremental vertical displacement.
¶$e_x(x_i, L/2)$ = incremental normal compressive strain.
¶q_d = incremental angle of uplift.